JACS
JOURNAL OF THE AMERICAN CHEMICAL SOCIETY

Article

pubs.acs.org/JACS

# Photocatalytic Conversion of Nitrobenzene to Aniline through Sequential Proton-Coupled One-Electron Transfers from a Cadmium Sulfide Quantum Dot

Stephen C. Jensen, Stephanie Bettis Homan, and Emily A. Weiss*

Department of Chemistry, Northwestern University, 2145 Sheridan Road, Evanston, Illinois 60208-3113, United States

Supporting Information

**ABSTRACT:** This paper describes the use of cadmium sulfide quantum dots (CdS QDs) as visible-light photocatalysts for the reduction of nitrobenzene to aniline through six sequential photoinduced, proton-coupled electron transfers. At pH 3.6–4.3, the internal quantum yield of photons-to-reducing electrons is 37.1% over 54 h of illumination, with no apparent decrease in catalyst activity. Monitoring of the QD exciton by transient absorption reveals that, for each step in the catalytic cycle, the sacrificial reductant, 3-mercaptopropionic acid, scavenges the excitonic hole in ~5 ps to form $QD^{\bullet-}$; electron transfer to nitrobenzene or the intermediates nitrosobenzene and phenylhydroxylamine then occurs on the nanosecond time scale. The rate constants for the single-electron transfer reactions are correlated with the driving forces for the corresponding proton-coupled electron transfers. This result suggests, but does not prove, that electron transfer, not proton transfer, is rate-limiting for these reactions. Nuclear magnetic resonance analysis of the QD–molecule systems shows that the photoproduct aniline, left unprotonated, serves as a poison for the QD catalyst by adsorbing to its surface. Performing the reaction at an acidic pH not only encourages aniline to desorb but also increases the probability of protonated intermediates; the latter effect probably ensures that recruitment of protons is not rate-limiting.

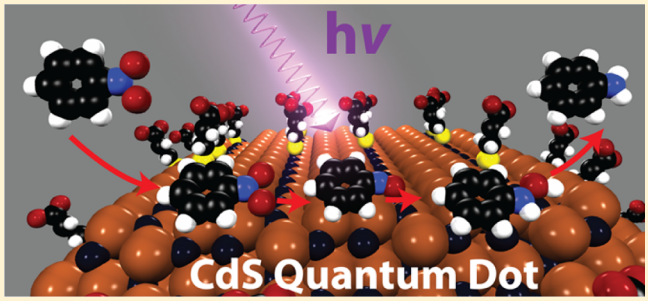


## INTRODUCTION

Direct band gap semiconductors used for heterogeneous photocatalysis are, with the proper passivating agents, more photostable and have higher extinction coefficients than the organic molecules and inorganic complexes typically used for homogeneous photocatalysis, over the range of visible and near-infrared energies relevant for solar energy conversion.[1−4] Bulk CdS, for example, is an active photocatalyst both for reactions that convert solar energy to liquid fuels and for photoinitiated small-molecule transformations.[5−14] On going from millimeter-sized particles to nanocrystals (with diameters of ~5 nm) of semiconductor, the surface-area-to-volume ratio increases by $\sim 10^6$. Furthermore, quantum confinement of excitons, which occurs when the size of the semiconductor crystal is on the order of or smaller than the Bohr radius of the exciton, increases both the oxidation and reduction potential of the semiconductor and enables tuning of these potentials (and the absorption spectrum) using the size of the colloid.[14] Photo-excited carriers in quantum-confined CdS (or CdS "quantum dots", QDs) have enough energy to perform many types of concerted reduction and oxidation reactions,[16] including both half-reactions for the photolysis of water,[2,17−20] and reduction of $CO_2$, for example to formic acid,[15] or CO.[21]

Multielectron photocatalysis is challenging, in part, because while a bulk or nanoparticle electrocatalyst under constant applied bias can perform concerted two-electron transfer steps, a photocatalyst under illumination with typical photon flux contains only a single exciton at any given time and therefore delivers only one electron at a time. In order to perform multielectron reactions, the photon-absorbing species (or "sensitizer") therefore must either (i) have a cocatalyst that efficiently accepts and accumulates charge carriers, (ii) have a mechanism to accumulate multiple charge carriers itself, or (iii) be able to stabilize one-electron intermediates long enough to re-establish its excited state, and possibly long enough to re-establish the catalyst–substrate encounter complex through diffusion. Quantum dots are effective sensitizers for metal-complex or enzyme cocatalysts (option i),[2,3,22−35] partially due to their long excited state lifetimes (tens of nanoseconds to microseconds),[36,37] which allow them to deliver charge carriers over long distances to weakly adsorbing species, and partially due to their tunable surface charge,[2,32,38,39] which allows for specific electrostatic interactions with, for instance, active sites on enzymes.[31,32,35] These specific interactions can lead to high selectivity by constraining the set of binding geometries of the catalyst or by increasing the rate of redox processes, leading to faster turnover and fewer side products' forming from idle intermediates.[35]

The high two-photon cross sections[40] and, in some cases, the ability to produce multiple excitons from one high-energy photon, a process called carrier multiplication,[41] may enable

**Received:** November 5, 2015
**Published:** January 19, 2016





DOI: 10.1021/jacs.5b11353
J. Am. Chem. Soc. 2016, 138, 1591–1600

QDs to accomplish multielectron transfer by accumulating multiple simultaneous redox equivalents itself (option ii). This option is exciting, but realizing it requires that substantial progress be made in stabilizing and extracting charge from the biexcitonic state before its decay.

Option iii, the stabilization of one-electron intermediates on the surface of the QD, is probably the most achievable route to the use of QDs as "direct" photocatalysts, where they act as both sensitizer and catalyst, for multielectron reactions. There are very few demonstrations[15,42] of the use of a QD as a direct photocatalyst for $CO_2$ or $H^+$ reduction, but it is somewhat more common in the oxidation[43,44] and the reduction[45−48] of non-$CO_2$ small-molecule organic substrates. Early studies documented the effective photoinitiation of the anionic polymerization of methyl methacrylate using ZnO QDs[49] and the polymerization of several vinylic monomers using CdS, ZnO, and $TiO_2$ QDs;[13] in these cases, quantum confinement of excitons was found to be essential to the catalysis. CdS QDs have been used for photoreduction of aromatic ketones,[10] methanol dehydrogenation,[11] and the two-electron reduction of benzophenone to benzhydrol.[12] The ability of QDs to couple single electron transfers to accomplish multielectron reactions was also highlighted in the catalysis of the two-electron oxidation reaction of 8-oxo-2′-deoxyguanosine and the six-electron reduction of nitrophenylalanine by CdSe QDs.[50]

Despite these demonstrations of the catalytic activity of QDs, the conditions under which the surface chemistry of the QD and the rates of elementary charge transfer steps permit QDs to perform proton-coupled multielectron reactions are still undefined, partially because the tools for quantitative analysis of QD surfaces are still in development.[51] Here, we begin to understand the mechanisms by which CdS QDs (diameter = 4.5 nm) are able to couple successive photoinitiated one-electron transfers to directly catalyze a six-electron, six-proton reduction of nitrobenzene (NB) to aniline (AN) in an acidic aqueous dispersion using 405 nm light (Scheme 1). This

**Scheme 1. QD Photocatalyzes the Reduction of Protonated Nitrobenzene ([NB H]$^+$) to Aniline ([AN H]$^+$) through Six Sequential Proton Coupled Electron Transfer Steps, with Nitrosobenzene ([NSB H]$^+$) and Phenylhydroxylamine ([PHA H]$^+$) Intermediates, and Using 3-Mercaptopropionic Acid (MPA) and MeOH as Proton and Terminal Electron Sources**[a]

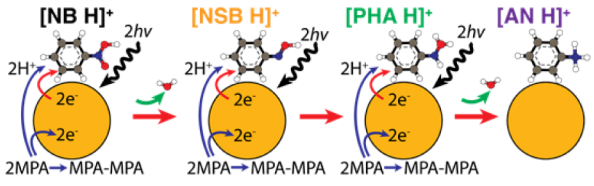


[a]Oxidation of MPA produces the corresponding disulfide ("MPA−MPA"). The text indicates the degree of protonation of each molecule at the pH of the reaction mixture (pH 3.6−4.3).

reaction is complicated but well-studied electrochemically[52] and is a good target reaction because it involves a series of small-molecule intermediates and photoproducts that can (i) be monitored by NMR and gas chromatography−mass spectrometry (GC−MS) and (ii) permeate the ligand shell of the QD and adsorb through either electrostatic or van der Waals interactions.[4,38,53] Our goal here is to identify some key parameters that control the efficiency of the reaction, not to optimize the performance of the catalyst, so we use a relatively low photon flux (7 mW) and only "buffer" the dispersion by controlling the concentration of excess 3-mercaptopropionic acid (MPA) that we add. Regardless, we achieve turnover rates of 23 electrons donated/QD/s, 4.3 NB molecules reduced/QD/s, and 2.6 AN molecules produced/QD/s. The QDs remain dispersed, and there is no detectable decrease in activity even after transferring $4.5 \times 10^6$ electrons per QD over 54 h.

Importantly, the low flux of photons used to continuously illuminate the catalytic reaction mixture dictates that one-electron intermediates, including protonated radicals of NB, nitrosobenzene (NSB), and phenylhydroxylamine (PHA), are stable for at least 7.1 ms in an 80:20 (v:v) $H_2O$:MeOH mixture at pH 3.6−4.3. An acidic pH is necessary for protonation of the product, aniline. Our NMR experiments show that aniline, unprotonated, binds to the surface of the QD and "poisons" the catalyst.

The solution dispersibility of the QD catalyst permits the in situ application of NMR and optical spectroscopy and facilitates mechanistic analysis of the system, including measurement of the rates of some of the elementary charge transfer steps within the catalytic cycle using transient absorption spectroscopy.[22,26,28,54,55]

## RESULTS AND DISCUSSION

The Supporting Information describes our procedure for synthesis and purification of oleate-capped CdS QDs with a first absorption peak at ∼407 nm and subsequent ligand exchange to form MPA-capped QDs. We perform the ligand exchange on small volumes of QDs, as needed, since the MPA-coated QDs are sensitive to oxygen and precipitate from solution over time.

**Preparation and Analysis of Catalytic Reaction Mixtures.** We prepare our samples by adding a mixture of 4 mM NB and 20 mM MPA to a 4 nM solution of MPA-capped CdS QDs in 80:20 $H_2O$:$CH_3OH$ and purging the solution for 3 min with Ar(g). Previous work on proton reduction has used ascorbic acid as both a source of protons and as a pseudobuffer that helps to maintain the acidic pH even as protons are reduced to hydrogen.[32] In this work, the excess, freely diffusing MPA serves as a pseudobuffer and a hole scavenger to regenerate the QD catalyst. It is convenient to use MPA for this purpose because it can also replace any ligands that desorb from the QD surface due to protonation or oxidation and thereby extend the lifetime of the catalyst.[3,32,56] We confirm that MPA serves as a source of electrons and protons by monitoring the formation of the corresponding disulfide, 3,3-dithiodipropionic acid, after illumination of the catalytic reaction mixture. These disulfides form even after exclusion of oxygen from the samples by Ar bubbling (see Figure S1 of the Supporting Information). A test experiment on a separate sample, however, shows that the MPA provides only ∼30% of the protons and electrons necessary to form the observed photoproducts (see the Supporting Information); this result suggests that the methanol cosolvent is also acting as a hole scavenger in this reaction. The oxidation potential of MPA and methanol are 0.35 and 0.48 V vs NHE, respectively,[57,58] so either may serve as a photoreductant for the QD.

We continuously illuminate the samples with a 405 nm, 7.0 mW laser with stirring. An autosampler injects the samples into an inlet at 250 °C, which evaporates the sample as neutral molecules that condense onto the column and is then linearly heated. NB desorbs from the column at 210 °C, in agreement


DOI: 10.1021/jacs.5b11353
J. Am. Chem. Soc. 2016, 138, 1591−1600

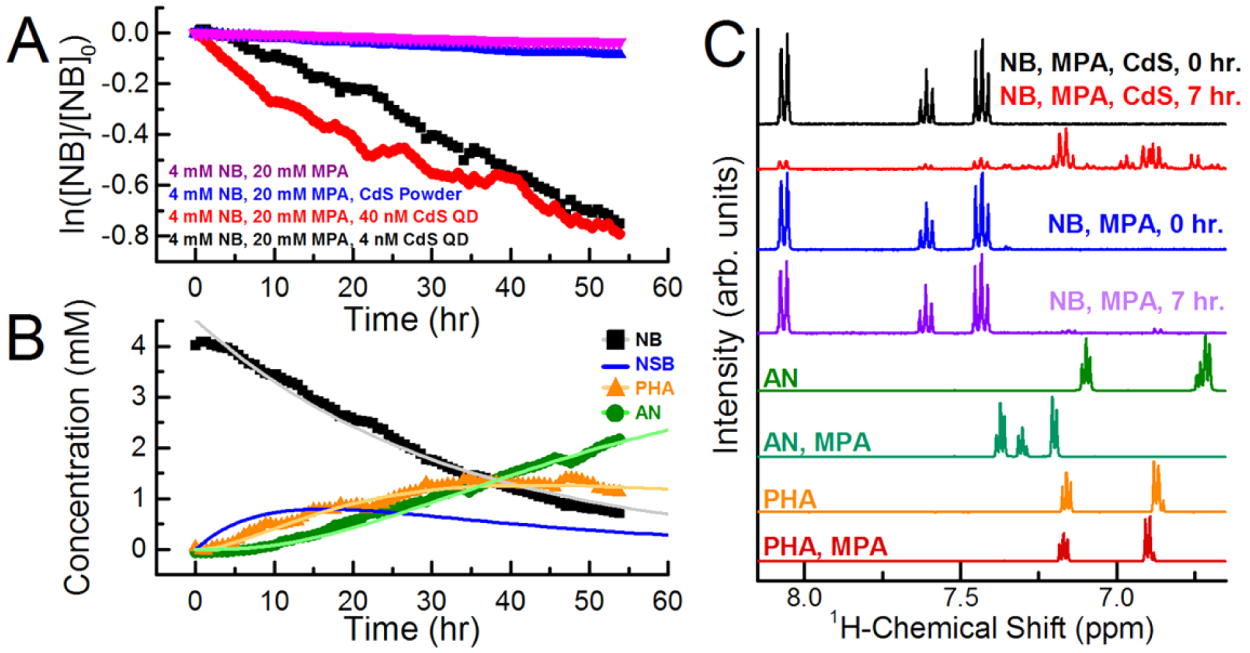


**Figure 1.** (A) The time-dependent concentration of nitrobenzene (NB), obtained from integrated GC spectra, within samples of NB and MPA (purple), or NB and MPA and 5 $\mu$g CdS powder (blue), or NB, MPA, and either 40 nM (red) or 4 nM (black) CdS QDs. All solutions are in 80:20 (v:v) $H_2O$:$CH_3OH$. The samples are purged with Ar(g) and illuminated with a 7 mW 405 nm laser with stirring. (B) The time-dependent concentration of NB (initially 4 mM) and reduction products PHA and AN in the presence of 20 mM MPA and 4 nM CdS QDs. The data is fit to a kinetic model of three sequential reactions described in the text (solid lines). The line corresponding to NSB is not measured directly but inferred from the kinetic model. (C) $^1$H NMR spectra of 4 mM NB and 16 mM MPA in 80:20 $D_2O$:$D_3OD$, with and without 40 nM CdS QDs, before and after 7 h of illumination with a 405 nm, 30 mW diode laser with stirring. Samples were purged with Ar(g) and allowed to sit for 30 min before the 0-h spectra were taken. The pH was 3.6 for all four NB samples. Also shown are spectra of control samples [4 mM AN (green) or PHA (orange)] and those compounds with 16 mM MPA (dark cyan and maroon, respectively). The triplet just upfield of 7.0 ppm in the spectrum of the reaction mixture (red) is unidentified, but it probably corresponds to a coupling product of a set of molecules in the reaction mixture; see the Supporting Information, Figure S4.

with its boiling point. We determine the concentration of NB by integrating the GC peak at $m/z$ = 123 and comparing it to the peak for an ethyl ether standard ($m/z$ = 74); see the Supporting Information, Figure S3.

**Kinetics and Yield of Nitrobenzene Degradation and Photoproduct Formation.** Figure 1A (black trace) shows that, in the presence of 4 nM CdS QDs and 20 mM 3-MPA, the NB concentration decays exponentially as a function of illumination time; we estimate a rate constant for NB degradation, which is pseudo-first-order with respect to the concentration of NB, of $-1.2 \times 10^{-2}$ h$^{-1}$ (black trace) for this decay by fitting the trace with a line. Without QDs (purple trace), there is some inefficient reduction of NB likely caused by the $H^+$-catalyzed photo-oxidation of MPA,[47] with a rate constant of $-6.6 \times 10^{-4}$ h$^{-1}$, a factor of 18.5 smaller than with the QD catalyst present. The rate constant for degradation of NB is a factor of 12.6 greater in the presence of CdS QDs than in the presence of a purchased CdS powder (blue trace). It is also a factor of 6.7 times greater than the reported rate constant for NB reduction in the presence of a CdS powder and cyclohexene as the hole scavenger[59] and a factor of 240 times greater than in the presence of CdS nanostructures with 2-propanol as the hole scavenger.[47] Increasing the concentration of QDs from 4 to 40 nM (red trace) while the initial concentration of NB is kept the same increases the initial decay rate constant by a factor of 3.4 (to $-2.8 \times 10^{-2}$ h$^{-1}$), but it does not increase the average rate constant over 54 h. The apparent decrease in the rate constant of NB degradation over time for the higher concentration of QDs probably results from the initially fast production of PHA and AN, which compete with NB for adsorption sites on the QD catalyst.

Figure 1B shows the time dependence of the photodegradation of 4 mM NB and the formation of PHA and AN photoproducts (measured by GC−MS; see the Supporting Information) under the same conditions as used to collect the black trace in Figure 1A, but plotted on a linear scale. As expected from previous cyclic voltammetry measurements,[60] we do not detect any NSB in these samples, by GC−MS or NMR. During the first ∼5 h of illumination, PHA is the majority product and the concentration of AN is below 10 $\mu$M. As the reaction proceeds and PHA reaches a maximum steady-state concentration of 1.4 mM, the AN concentration increases linearly.

The GC-measured time traces for NB, PHA, and AN can be globally fit with the equations derived from a simple kinetic model of three sequential reactions (NB → NSB → PHA → AN), where we assert that the second reaction is irreversible to account for the absence of NSB in the steady state. This fit yields reasonable rate constants for each two-electron step (see the Supporting Information). Although we cannot directly detect NSB, the model predicts that the concentration of NSB peaks after ∼10 h and decreases (blue trace in Figure 1B) due to the fixed amount of NB present in the system over the course of the experiment. The concentration of PHA, which is formed from NSB, peaks at ∼33 h and then decreases as the availability of NSB decreases.

$^1$H NMR spectra of the illuminated reaction mixtures are sensitive to the protonation states of the molecules and show


DOI: 10.1021/jacs.5b11353
J. Am. Chem. Soc. 2016, 138, 1591−1600

that photoreduction of $[NB\ H]^+$ forms a mixture of AN and $[AN\ H]^+$ through a mixture of PHA and $[PHA\ H]^+$ intermediates (Figure 1C and Figure S1 of the Supporting Information). This result is reasonable because the pH of these samples was 3.6, at which, based on the respective $pK_a$ values of their protonated forms in pure water,[61] 60% of NB molecules, 40% of NSB molecules, 17% of PHA molecules, and 79% of AN molecules should be protonated (see the Supporting Information). Integration of the peaks in the GC spectra for all species before and after illumination demonstrates that the total intensity of aromatic protons in these reaction mixtures is conserved during the reaction.

By 54 h, each QD has donated an average of 4.5 million electrons to reduce 825 000 $[NB\ H]^+$ molecules to 500 000 $[AN\ H]^+$ and 325 000 $[PHA\ H]^+$ molecules per QD. After 54 h of illumination, the first absorption peak of the QDs is still present, and the QDs are still emissive from the band edge, but a lower-energy, broadened emission feature appears (see the Supporting Information, Figure S4). We have not conclusively identified this feature, but we believe that it is due to formation of a fluorescent coupling product (or products, such as azobenzene) between one or more sets of compounds in the reaction mixture, possibly catalyzed by the QD.[62] The presence of this compound does not appear to affect the catalytic activity of the QDs for NB reduction.

The internal quantum efficiency of photon-to-electron conversion for this system at 405 nm, measured by GC–MS, is 1.9% for the four-electron process to form PHA and 37.1% per electron transfer step. Previously, NB has been photoreduced to PHA through direct excitation with 366 nm light using 2-propanol as the hole acceptor, with an internal quantum efficiency of 30% per electron transfer step.[63]

Figure 2 shows that the CdS QDs are the active sensitizers for the reduction of NB. To construct this figure, we prepared eight identical vials with 4 mM NB, 20 mM MPA, and 4.0 $\mu$M CdS QDs. We illuminated each sample for 4 min at one of eight wavelengths between 360 and 452 nm centered around the first absorption peak of the QDs (415 nm), with a commercial Ti–sapphire laser (Spitfire, 1 kHz, 100 fs, Spectra Physics) guided into an optical parametric amplifier (TOPAS-C, Light Conversion). The lowest energy transition for NB itself is an n → $\pi^*$ transition that occurs at 340 nm,[63] so we do not directly excite the NB with this range of wavelengths. To simplify our analysis, we only illuminated the sample for 4 min, at which point PHA is the only stable photoproduct and accounts for all of the electrons donated by the QDs (see the Supporting Information, Figure S2). At each wavelength, we measured the number of PHA molecules detected per incident photon by integrating the area of its phenyl ring protons in the NMR spectrum of the mixture and comparing it to a calibration curve for PHA (see the Supporting Information). This action spectrum overlays the ground-state absorption spectrum of the QDs, so we conclude that the reducing electrons for this reaction originate from the excitonic states of the QD.

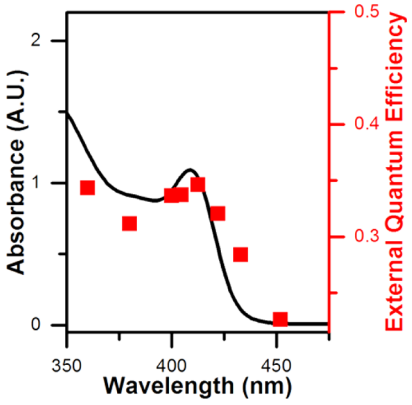


**Figure 2.** Per photon external quantum efficiency (EQE) of NB to PHA formation of CdS QDs (right axis, red squares) overlaid on the QDs' measured absorption spectrum (left axis, black line). To obtain the action spectrum, eight reaction mixtures of 4.0 $\mu$M CdS QDs, 0.4 mM NB, and 20 mM 3-MPA in 80:20 $D_2O$:$D_3OD$ were illuminated for 4 min by a ~5 mW laser tuned to each wavelength. A separate control confirms that no PHA is formed without light. All samples have a volume of 1.0 mL and are degassed by bubbling with Ar(g) for 4 min. The EQE is calculated by dividing the total number of PHA molecules produced, measured by $^1$H NMR, by the number of incident photons. At this QD concentration (4.0 $\mu$M), 100% of incident photons are absorbed, so the EQE ~ IQE as measured by GC–MS on a less-concentrated sample (37.1%).

**Mechanism for the Photocatalytic Reduction of Nitrobenzene to Aniline by CdS QDs.** The multistep reduction of NB to AN requires a total of six electrons and protons and occurs through NSB and PHA intermediates. In a 1:1 $H_2O$:MeOH mixture, the potential for the $2e^-$, $2H^+$ reduction of NB to NSB, with elimination of water, is −0.16 V vs NHE), the potential for the $2e^-$, $2H^+$ reduction of NSB to PHA is +0.29 V vs NHE, and the potential for the $2e^-$, $2H^+$ reduction of PHA to AN, with elimination of water, is −0.46 V vs NHE.[60] Since the formation of each $2e^-$ intermediate is detected electrochemically as a concerted two-electron step (with a single current peak for each step), we equate the $2e^-$, $2H^+$ reduction potentials with the $1e^-$, $1H^+$ reduction potentials. All of these potentials are lower than that of electrons in the LUMO (lowest state of the conduction band) of a 4.5 nm CdS QD, the potential of which has been measured to be as high as −2.0 V vs NHE.[64] The electron transfer to each substrate therefore can occur spontaneously upon photoexcitation of the QD. The NSB intermediate is easier to reduce than NB, so without trapping by a nucleophile, NSB is typically not observed, and the reaction of NB to PHA is detected as a single four-electron transfer step.[52,60,65]

With the aid of our data in Figure 1 and the proposed mechanisms of Bard and others,[52,65] we outline the photocatalytic cycle from NB to AN under acidic conditions in Scheme 2. For clarity, we show the protonated forms of all reagents and products, but as mentioned previously, at the measured pH of 3.6, we have mixtures of protonated and unprotonated NB, NSB, PHA, and AN.

Unlike other published mechanisms, the cycle in Scheme 2 includes plausible one-electron intermediates that are not observed in the electrocatalysis experiment. We include these intermediates because, given the flux of photons into the system ($4.6 \times 10^{17}$ photons $cm^{-2}$ $s^{-1}$), the absorption coefficient of the QDs (which dictates that they absorb 1.1% of incident photons), and the excited state lifetime of the QDs without added NB, each QD contains one exciton or fewer at any given time and, therefore, only delivers one electron at a time. Furthermore, this photon flux dictates that the lifetime of each one-electron intermediate shown in Scheme 2 must be at least 7.1 ms such that it can be converted, upon creation of the next exciton in the QD, to the two-electron product (see the Supporting Information for this calculation).


DOI: 10.1021/jacs.5b11353
J. Am. Chem. Soc. 2016, 138, 1591–1600

**Scheme 2. Catalytic Cycle for the Six-Electron, Six-Proton Photoreduction of Nitrobenzene (NB, 1) to Aniline (AN) through Nitrosobenzene (NSB, 2) and Phenylhydroxylamine (PHA, 3) Two-Electron Intermediates, All of Which Are Partially Protonated at pH 3.6**[a]

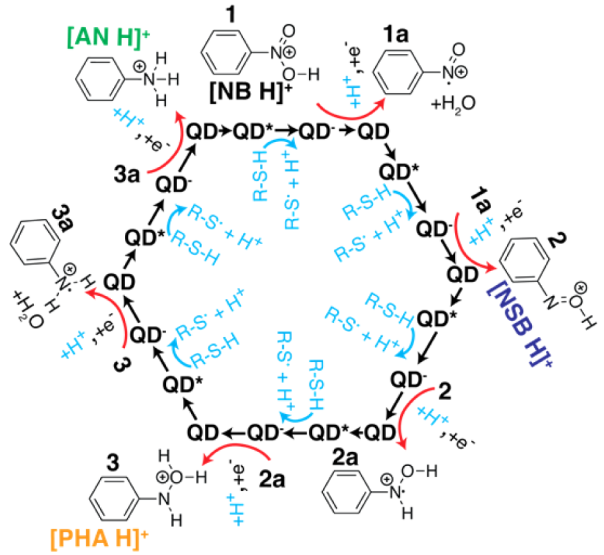


[a]3-Mercaptopropionic acid (R−S−H) serves as a sacrificial reductant to regenerate the CdS QD catalyst, but it cannot account for all of the protons and electrons used in the reaction, some of which are probably provided by the MeOH cosolvent. **1a**, **2a**, and **3a** denote proposed one-electron intermediates formed during the cycle.

**Analysis of the Adsorption of Reagents and Photoproducts to the Surface of QDs.** In order to determine whether the reactions with the cycle depicted in Scheme 2 occur within temporary encounter complexes of freely diffusing QDs and molecules or whether the molecules are statically adsorbed to the QDs, we measured, by NMR, the number of NB, NSB, PHA, and AN molecules that adsorb to each QD under acidic conditions (pH ∼5). Molecules bound to nanoparticles have a large rotational correlation time, which broadens the NMR resonance for protons close to the QD and makes it difficult to distinguish the signal from the baseline noise. The degree of broadening scales with the fraction of time that the molecule is adsorbed to the QD, as well as the size and rigidity of the molecule. If the broadening upon adsorption is dramatic enough, the molecules becomes NMR-invisible.[51,66−68] We can therefore estimate the number of bound molecules per QD by monitoring the decrease in the integrations of their NMR signals upon mixing them with QDs. Table 1 lists the average number of NB, NSB, PHA, and AN molecules bound per QD in mixtures of 0.4 mM of each of the molecules with 4.0 μM QDs (where the molecules were added directly, not produced by reaction of NB) and the corresponding adsorption constants. We acquired NMR spectra of these samples after 1 h of stirring in the dark. For comparison, we also list the data for samples without excess MPA (pH ∼9.0 due to the presence of Triton B), at which pH the unprotonated forms of NB, NSB, PHA, and AN dominate.

From the data in Table 1, we conclude that protonation does not affect the binding constant of NB ($pK_a$ ∼ 4.0), but it decreases the binding constant of AN ($pK_a$ ∼ 4.6) by approximately a factor of 6, probably because of a large increase in the solubility of AN in water once protonated.[61] On

**Table 1. Number of Bound Molecules per QD as a Function of MPA Concentration**[a]

| | no MPA (pH ∼9) | | 15 mM MPA (pH ∼5) | |
|---|---|---|---|---|
| | molecules bound per QD | $K_{ads}$ = [bound]/[free] | molecules bound per QD | $K_{ads}$ = [bound]/[free] |
| NB | 80.5 ± 8.9 | 0.81 ± 0.09 | 80.3 ± 1.2 | 0.80 ± 0.01 |
| NSB | 41.3 ± 2.2 | 0.41 ± 0.02 | 77.9 ± 2.7 | 0.78 ± 0.03 |
| PHA | 79.3 ± 1.6 | 0.79 ± 0.02 | 72.0 ± 5.5 | 0.72 ± 0.05 |
| AN | 82.1 ± 2.2 | 0.82 ± 0.02 | 13.5 ± 2.4 | 0.13 ± 0.02 |

[a]Measured by $^1$H NMR on samples comprising 0.4 mM of each molecule with 4.0 μM QDs and stirred for 1 h before measurement (see the Supporting Information, Figure S5). The errors are the standard deviations from three measurements on three separately prepared samples.

going from pH 9 to pH 5, we only change the number of protonated PHA molecules ($pK_a$ ∼ 1.9) from 0.1% to 4.7%, so we do not significantly affect their average solubility or affinity for the QD surface. Interestingly, the binding constant of the QD−NSB complex increases by approximately a factor of 2 on going from <1% protonated NSB at pH 9 to 14% protonated NSB at pH 5. The binding constant of a QD−molecule complex depends on a number of factors, including the solubility of the molecule in the surrounding solvent and the magnitude of electrostatic and van der Waals interactions with the QD core and the ligand shell. We cannot, with our current data set, assess the respective contributions of these factors to the data in Table 1. Given, however, that the maximum number of molecules that adsorb to the QDs (under the two pH values we examined) is ∼80 for all four molecules, we can conclude that there exist approximately 80 binding sites for molecules of this size on the surface of the QD. Furthermore, the fact that ∼80 NB, NSB, and PHA molecules are bound at acidic pH implies that under the conditions used to gather the data in Figure 1, there is no incentive for the catalytic substrate to desorb from the QD surface until AN is formed. We therefore tentatively conclude that all steps in the catalytic cycle occur through "static" proton-coupled electron transfer reactions from QDs to preadsorbed molecules and are not diffusion-controlled. These data also suggest one reason why, when excess MPA is not present, the number of catalytic turnovers (over 54 h) decreases by a factor of ∼2; under neutral or basic conditions, AN saturates the QD surface and leaves no room for NB to adsorb and thereby poisons the catalyst.

**Measurement of the Rates of Some Elementary Electron and Hole Transfer Steps.** Figure 3A shows the transient absorption (TA) spectrum of a sample of 2 μM CdS QDs (no added NB or excess MPA) in 80:20 $H_2O$:MeOH, collected 1 ns after excitation at 390 nm. The main feature in this spectrum is the bleach of the ground-state absorption centered at 413 nm. This bleach reflects the depopulation of the ground state by the 390 nm pump laser. It forms on the time scale of photon absorption and recovers as the excitonic electron leaves the conduction band of the QD core, here by electron transfer to NB, NSB, or PHA. We monitor electron dynamics at 420 nm (marked with a red dotted line), rather than the center of the bleach, because, at shorter wavelengths, scatter from the pump laser contaminates the signal. The ground-state bleach signal of cadmium chalcogenide QDs is not sensitive to the location or dynamics of the excitonic hole because of the high near-degeneracy of valence band-edge states compared to conduction band-edge states.[69−72] We


DOI: 10.1021/jacs.5b11353
J. Am. Chem. Soc. 2016, 138, 1591−1600

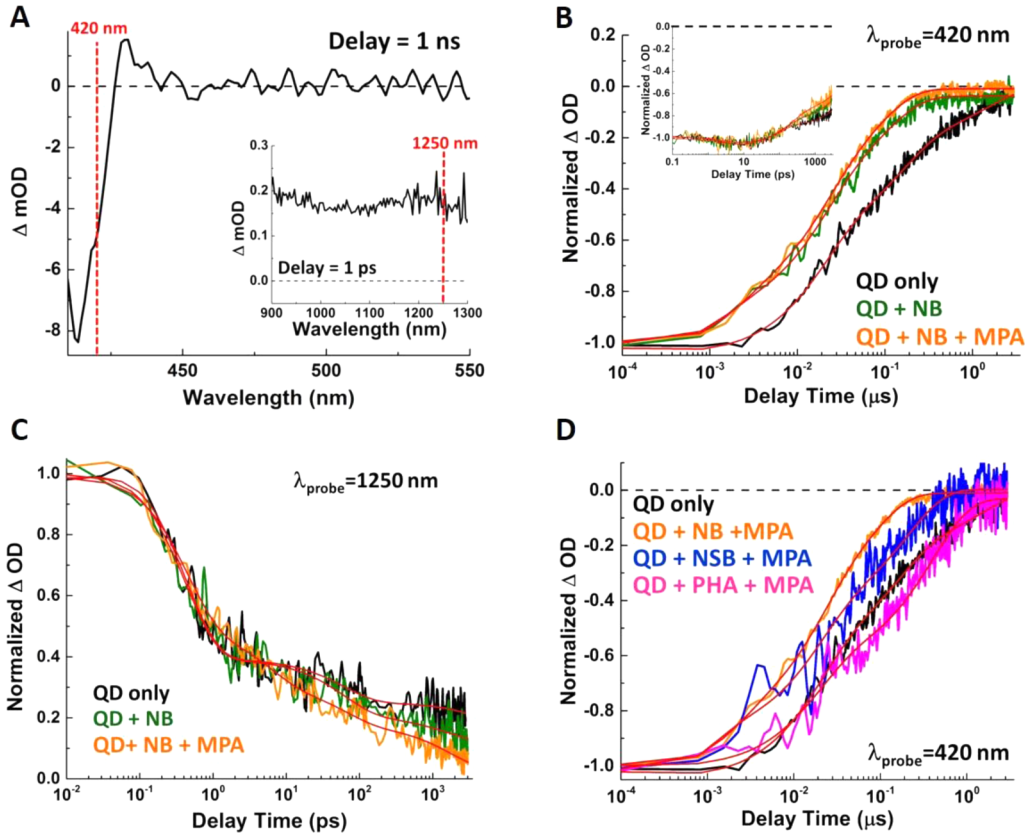


**Figure 3.** (A) Visible TA spectrum of 2 $\mu$M CdS QDs (no added NB or excess MPA) in 80:20 $H_2O$:MeOH, collected 1 ns after excitation at 390 nm. Inset: Near-infrared TA spectrum of the same sample of CdS QDs collected 1 ps after excitation at 390 nm. The red dotted lines mark two of the wavelengths at which we monitored the dynamics of the excited state of the QD, as shown in parts B–D. (B) Normalized kinetic traces, monitored on the nanosecond-to-microsecond time scale, extracted at 420 nm from the TA spectra of the 2 $\mu$M QDs (black), the QDs with 1000 eq of NB (green), and the QDs with 1000 eq of NB and 1000 eq of 3-MPA (orange). Inset: Normalized kinetic traces extracted at 420 nm from the TA spectra of the same samples, but monitored on the ultrafast time scale (150 fs–3 ns). Signals at 420 nm are dominated by the dynamics of the excitonic electron. (C) Normalized kinetic traces, monitored on the ultrafast time scale, extracted at 1250 nm from the TA spectra of the same samples as in part B. Signals at 1250 nm are dominated by the dynamics of the excitonic hole. (D) Normalized kinetic traces, monitored on the nanosecond-to-microsecond time scale, extracted at 420 nm from the TA spectra of the QDs (black), the QDs with 1000 eq of NB and 1000 eq of 3-MPA (orange), the QDs with 1000 eq of NSB and 1000 eq of 3-MPA (blue), and the QDs with 1000 eq of PHA and 1000 eq of 3-MPA (pink).

**Table 2. Time Constants for Excited-State Decay of CdS QDs with Various Photoxidants and the Photoreductant MPA**[a]

| | $\tau_1$,[b] fs ($A_1$) | $\tau_2$,[b] ps ($A_2$) | $\tau_3$,[b] ps ($A_3$) | $\tau_4$,[c] ns ($A_4$) | $\tau_5$,[c] ns ($A_5$) | $\tau_6$,[c] ns ($A_6$) | $\tau_7$,[c] $\mu$s ($A_7$) |
|---|---|---|---|---|---|---|---|
| | $h^+$ trapping | $h^+$ transfer to MPA | $h^+$ trapping | $e^-$ transfer to photo-oxidant | radiative CR ($e^- + h^+$) | CR of $e^-$ with trapped hole | CR of $e^-$ with trapped hole |
| QD | 440 ± 32 (0.87) | – | 63 ± 10 (0.13) | – | 18 ± 1 (−0.45) | 154 ± 11 (−0.35) | 1.6 ± 0.1 (−0.20) |
| QD–NB | 440 (0.84) | – | 63 (0.16) | **1.1 ± 0.5** (−0.33) | 18 (−0.36) | 101 ± 4 (−0.28) | offset[d] (−0.03) |
| QD–[NB H]$^+$ + MPA | 440 (0.71) | **5.7 ± 1.0** (0.17) | 63 (0.12) | **1.7 ± 0.3** (−0.31) | 18 (−0.37) | 82 ± 2 (−0.31) | offset[d] (−0.01) |
| QD–[NSB H]$^+$ + MPA | not measured | not measured | not measured | **0.82 ± 0.94** (−0.44) | 18 (−0.28) | 208 ± 11 (−0.28) | offset[d] (0.002) |
| QD–[PHA H]$^+$ + MPA | not measured | not measured | not measured | – | 18 (−0.39) | 406 ± 14 (−0.58) | offset[d] (−0.03) |

[a]Lifetimes in bold are those that are not found in the QD-only sample. Each lifetime is the average of two measurements on separately prepared samples that differed by less than 50%. The quantities in parentheses are the fractional amplitudes of each component at each probe wavelength: $A_1 + A_2 + A_3 = 1$ and $A_4 + A_5 + A_6 + A_7 = 1$. [b]Monitored at $\lambda_{probe}$ = 1250 nm. [c]Monitored at $\lambda_{probe}$ = 420 nm. [d]Fit as a constant $y$-offset rather than an exponential decay of the signal because the decay is too slow to measure on this time scale.

instead monitor the hole at 1250 nm (Figure 3A, inset), where, for CdSe QDs, it is known that the dynamics of the TA signal are dominated by the dynamics of the excitonic hole.[69] Indeed, we observe dynamics at 1250 nm that we do not observe at 420 nm; it is these dynamics that we attribute to the excitonic hole (see the Supporting Information).

Figure 3B shows the dynamics of the excitonic electron, monitored at 420 nm, for the QD, the QD plus 1000 equiv of NB, and the QD plus 1000 eq of both NB and MPA. The time scale we focus on here is 0.1 ns to 1 $\mu$s, because the TA signal at this wavelength does not begin to change until ~100 ps after photoexcitation (see Figure 3B, inset), so the dynamics are


DOI: 10.1021/jacs.5b11353
J. Am. Chem. Soc. 2016, 138, 1591–1600

Table 3. Summary of the Measured Intrinsic Rate Constants for One-Electron Transfers from $QD^-$ (Scheme 2)

| electron acceptor (X) | reduction potential of X (V vs NHE) | $k_{eT,int}$ ($s^{-1}$) for the reaction $QD^- + X \rightarrow QD + X^-$ |
|---|---|---|
| $[NB\ H]^+$ | −0.16 | $7.3 \times 10^6$ |
| $[NSB\ H]^+$ | +0.29 | $1.6 \times 10^7$ |
| $[PHA\ H]^+$ | −0.46 | $<3.4 \times 10^4$ |

more accurately monitored and fit on the nanosecond time scale. We fit the kinetic traces in Figure 3B using a sum of simple exponential components convoluted with an instrument response function (see the Supporting Information). The kinetic trace for the QD-only sample (black) fits to a sum of three exponential components with time constants of 18 ns, 154 ns, and 1.6 μs ($\tau_5$, $\tau_6$, and $\tau_7$, respectively, in Table 2). On the basis of extensive previous work on exciton dynamics in cadmium chalcogenide QDs[69−72] and the fact that we know the dynamics are specific to the excitonic electron, we assign the 18 ns component to radiative recombination and the two longer components to recombination of the excitonic electron with a surface or lattice-trapped hole. When fitting the kinetic traces corresponding to the samples of QDs mixed with NB (green) or NB and MPA (orange), we find that, in addition to the components needed to fit the kinetic trace for the QDs alone, a component with either $\tau$ = 1.1 ns (green) or $\tau$ = 1.7 ns (orange) is needed to adequately fit the kinetic trace (these time constants are listed as "$\tau_4$" in Table 2). We assign this time constant in both cases to transfer of the photoexcited electron to NB.

The slight discrepancy between the time constants for electron transfer from a photoexcited CdS QD to NB with excess MPA (1.7 ns) and without excess MPA (1.1 ns) could be due to the different protonation states of NB under those two conditions. Alternatively, it could be due to the fact that, when excess MPA is present, it scavenges the excitonic hole of the QD to form $QD^{\bullet-}$, which then is the electron donor to NB. When MPA is not present, the excited state of the QD, QD*, is the electron donor.

We obtain the dynamics of the hole transfer process from the dynamics in Figure 3C, which shows kinetic traces extracted from the TA spectra of the same samples as in Figure 3B, but monitored at 1250 nm. The dynamic components at 1250 nm attributable to photoinduced intraband transitions of the excitonic hole are those components that are not present in dynamics of the ground-state bleach (for more details, see Figure S10 and Table S3 of the Supporting Information). Fits to these kinetic traces show that hole transfer from a photoexcited CdS QD to MPA occurs in 5.7 ps ($\tau_2$ in Table 2), prior to the electron transfer process. This order of events is reflected in the catalytic cycle in Scheme 2. The 5.7 ps component is needed to adequately fit the kinetic trace for the sample of QDs plus NB and MPA, but it is not needed to fit the traces for the samples of QDs alone or QDs plus NB. We therefore conclude that it is the excess MPA in solution, not the MPA bound to the QD (which is present in all three samples), that is responsible for the hole scavenging. We suspect that we do not observe the hole transfer process in the presence of MeOH without excess MPA because MeOH scavenges holes from surface traps on the QD surface, rather than holes from the QD core; the signal at 1250 nm is not sensitive to the dynamics of surface-trapped holes. The dynamics in Figure 3C also show the presence of two other pathways with time constants of 440 fs and 63 ps. These processes are seen in all three samples (Table 2), have time constants that correspond to those observed for decay of excitons in CdSe QDs[69] and are assigned to trapping of the hole to a lattice chalcogenide (<1 ps) and trapping of the hole to a surface chalcogenide (∼50 ps).

Figure 3D shows the same type of data as Figure 3B, the dynamics of the photoexcited electron monitored at 420 nm, for a QD-only sample and for samples of QDs mixed with NB, NSB, or PHA. All samples have excess MPA, in order to best simulate the conditions of the catalysis. The time constant for electron transfer from the QD to $[NSB\ H]^+$ (∼0.8 ns) is shorter than that for electron transfer from the QD to $[NB\ H]^+$ (∼1.7 ns). Both of these time constants are longer than most measured electron transfer time constants from CdS QDs to adsorbed acceptors,[73−75] but they are too short to reflect a diffusion-limited electron transfer process, which, based on the collision frequency, has a minimum value of 30 ns for this system (see the Supporting Information). This result supports our tentative conclusion from the NMR adsorption experiment that electron transfer in these systems occurs within statically adsorbed QD−molecule complexes.

The time constant for electron transfer from the QD to $[PHA\ H]^+$ is much longer than that for the other two substrates. In fact, in the case of the QD−PHA sample, we cannot deconvolute the electron transfer time constant from one of the electron trapping time constants, so we can only conclude that this time constant is on the 100 ns time scale. This time constant could, in principle, reflect a diffusion-limited process, but on the basis of the NMR result that, under acidic conditions, $[PHA\ H]^+$ has a very similar affinity for the QD surface to those of $[NB\ H]^+$ and $[NSB\ H]^+$, we can reasonably conclude that the relatively slow electron transfer to $[PHA\ H]^+$ is due to (i) the smaller driving force for its reduction (discussed below) or (ii) the contribution of proton transfer to the observed rate, since, at pH 3.6, only 17% of PHA molecules are protonated (as opposed to 60% of NB and 40% of NSB).

In order to physically interpret the trend in rate constants for electron transfer to the catalytic substrates, we must convert the observed rate constant to the "intrinsic" rate constant, $k_{eT,int}$, for each reaction. Observed rate constants for charge separation between QDs and molecules scale linearly with the number of electron-accepting molecules bound per QD. The intrinsic rate constant is the single donor−single acceptor rate constant, which is the number that is correlated with the driving force and electronic coupling for the electron transfer reaction through the Marcus equation.[74] The intrinsic rate constant is simply the observed rate constant divided by the number of adsorbed acceptors per QD, which we estimate from the NMR data in Table 2. The values of $k_{eT,int}$ are $7.3 \times 10^6\ s^{-1}$ for the QD−$[NB\ H]^+$ donor−acceptor pair, $1.6 \times 10^7\ s^{-1}$ for the QD−$[NSB\ H]^+$ pair, and $<3.4 \times 10^4\ s^{-1}$ for the QD−$[PHA\ H]^+$ pair (Table 3).

The rate constants for electron transfer—$k_{eT,int}$(QD−$[NSB\ H]^+$) > $k_{eT,int}$(QD−$[NB\ H]^+$) > $k_{eT,int}$(QD−$[PHA\ H]^+$)—are correlated with the magnitudes of the driving forces for the corresponding proton-coupled two-electron reactions: $|\Delta G_{eT}$(QD−$[NSB\ H]^+$)| > $|\Delta G_{eT}$(QD−$[NB\ H]^+$)| >


DOI: 10.1021/jacs.5b11353
J. Am. Chem. Soc. 2016, 138, 1591−1600

$|\Delta G_{eT}(QD-[PHA\ H]^{+})|$.[60] These driving forces are best approximated as the reduction potential of the QD, which has been reported in the range from −0.8 to −2.0 V vs NHE,[64,76,77] minus the reduction potential of the substrate (+0.29 V vs NHE for NSB, −0.16 V vs NHE for NB, and −0.46 V vs NHE for PHA),[60] since the electron transfer occurs from the QD anion (formed upon scavenging of the hole by MPA) to the substrate. This correspondence between the rate constant and thermodynamic driving force is not necessarily expected, since the TA measures the rate of the one-electron reaction and the potentials we quoted are for the two-electron reaction and since recruitment of protons for these reactions could contribute to an overpotential that would influence the observed rate. If this correlation is, in fact, physically meaningful, it indicates that (i) the driving forces for each electron transfer within a two-electron step are very similar (a result corroborated by cyclic voltammetry[60]) and (ii) electron transfer, rather than proton transfer, is rate-limiting, a result that has been reported once previously in the context of direct catalysis of proton reduction by a CdSe QD.[42] This result could be due to a high concentration of protons at the QD surface. We are cautious with our interpretation of the trend in rate constants, however, because we do not know the absolute values of the driving forces (due to the uncertainty in the reduction potential for the QDs) nor the reorganization energy for these reactions; therefore, we do not know whether the reactions are in the Marcus normal or inverted region. This information is crucial in determining the rate-limiting steps of the catalytic cycle.

We also estimated, from the amplitudes of the electron transfer components in the TA spectra, the internal quantum yield of electron transfer from the QD to NB (0.31) and to NSB (0.44). The average amplitude of 0.38 agrees well with the average internal quantum yield we independently measure with GC−MS (0.37) and in constructing the action spectrum in Figure 2 (0.34 at 400 nm).

## CONCLUSION

In this work we demonstrate that CdS QDs are an active photocatalyst for the six-electron, six-proton reduction of nitrobenzene (NB) to aniline (AN) through a series of photoinduced one-electron transfers and nitrosobenzene (NSB) and phenylhydroxylamine (PHA) intermediates. At an excitation wavelength of 405 nm, the internal quantum efficiency of conversion of photons to reducing electrons is 37%. Transient absorption measurements show that each catalytic step occurs first by hole transfer from the photoexcited QD to 3-mercaptopropionic acid (which is present in solution in excess) in 5.7 ps to form $QD^{\bullet-}$; the negatively charged QD then donates an electron to an adsorbed substrate molecule on the nanosecond time scale. The rate constant for each electron transfer step is correlated with the driving force for the corresponding two-electron, two-proton reduction, which is consistent with the observation of concerted two-electron steps in the electrocatalysis of this reaction and, more importantly, implies that electron transfer, and not proton transfer, is the rate-limiting step for each reduction. A more definitive conclusion about rate-limiting steps, however, requires knowledge of the absolute values of (not just trend in) driving forces and the values of reorganization energy for these reactions.

Acidic conditions play a significant role in the success of this reaction. A pH of ∼4 ensures that a large percentage of NB, NSB, and AN molecules are protonated. For nitrosobenzene, NMR studies reveal that protonation enhances the adsorption constant by a factor of ∼2, while NB and PHA (which is only 17% protonated at pH ∼3.6) both have a high affinity for the QD surface regardless of protonation state. Adsorption of the reagents to the QD surface throughout the catalytic cycle ensures that the reaction never becomes diffusion-controlled. Protonation decreases the adsorption constant of AN such that it desorbs to make room for another NB molecule. Furthermore, a supply of protons at the QD surface—it is possible that the local concentration of protons at the QD surface is higher than in the bulk because of the negatively charged MPA ligands—may ensure that proton transfer is not a rate-limiting step. It would be useful to examine the pH-dependence in either the catalytic yield or electron transfer rates. In this study, however, the pH affects several variables, including the protonation state of the substrate, protonation state of MPA (and therefore the electrostatic interactions at the QD surface), and the number of available binding sites (and therefore the statistical enhancement of the observed electron transfer rate). Deconvoluting these factors is beyond the scope of this work, but it is an issue that we plan to address in future studies.

The high photocatalytic activity of the QDs for this particular reaction is probably also related to the small size of the catalytic substrates. They are small enough to permeate the ligand shell and find ∼80 adsorption sites per QD. We facilitate the substrate−surface interaction by exchanging the native oleate ligands with short MPA ligands.[14,78] The QD surface may also enable the surprising stability of the one-electron radical intermediates, which must exist given our low photon flux. The stability of these intermediates could come from the polar QD surface or from the negatively charged MPA ligands.

Finally, as has been seen previously,[23,55,79,80] fast hole scavenging from the photoexcited QD is a critical part of this catalytic cycle; it allows the reducing electron to exist long enough to perform the slow reduction of phenylhydroxylamine to aniline. The fast observed rate of hole extraction in this system is probably due to the large number of available hole transfer pathways (i.e., the large number of proximate MPA molecules) per QD, since the intrinsic rate of hole extraction from cadmium chalcogenide QDs is typically a factor of 10−100 slower than what we measure here.[81]

Clearly, there is still much to understand about the mechanisms of multielectron, proton-coupled reactions mediated by the surfaces of nanostructures. This work shows that semiconductor quantum dots are, at worst, an excellent model system for discovery in this area and, at best, the next great class of high-performing photocatalysts.

## ASSOCIATED CONTENT

### Supporting Information

The Supporting Information is available free of charge on the ACS Publications website at DOI: 10.1021/jacs.5b11353.

Procedure for the synthesis/purification of the QDs; additional $^{1}H$ NMR spectra; details of NB, PHA, and AN quantification from GC−MS; spectra of QDs after illumination; DOSY NMR measurements of diffusion constants; additional calculations; photoluminescence quenching of CdS QDs in the presence of NB; and kinetic traces of excited state decay of CdS QDs with NB and MPA (PDF)



DOI: 10.1021/jacs.5b11353
J. Am. Chem. Soc. 2016, 138, 1591−1600

## AUTHOR INFORMATION


### Corresponding Author

*e-weiss@northwestern.edu


### Notes

The authors declare no competing financial interest.

## ACKNOWLEDGMENTS

This work was supported as part of the Argonne-Northwestern Solar Energy Research (ANSER) Center, an Energy Frontier Research Center funded by the U.S. Department of Energy, Office of Science, Basic Energy Sciences under Award # DE-SC0001059. Initial catalyst development was conducted with support by the Army Research Office via the Presidential Early Career Award for Scientists and Engineers (PECASE) to E.A.W. GC−MS and NMR data were acquired at Northwestern University's Integrated Molecular Structure Education and Research Center (IMSERC). S.C.J. thanks the Northwestern International Institute for Nanotechnology (I.I.N.) for a postdoctoral fellowship. The authors thank Dr. Igor Dubovyk and Prof. Regan Thomson for helpful discussions.

## REFERENCES


(1) Gould, T. J.; Hess, S. T.; Bewersdorf, J. *Z. Phys. Chem.* **2008**, *222*, 833.
(2) Yehezkeli, O.; de Oliveira, D. R. B.; Cha, J. N. *Small* **2015**, *11*, 668.
(3) Das, A.; Han, Z. J.; Haghighi, M. G.; Eisenberg, R. *Proc. Natl. Acad. Sci. U. S. A.* **2013**, *110*, 16716.
(4) Yu, W. W.; Qu, L.; Guo, W.; Peng, X. *Chem. Mater.* **2003**, *15*, 2854.
(5) Dukovic, G.; Merkle, M. G.; Nelson, J. H.; Hughes, S. M.; Alivisatos, A. P. *Adv. Mater.* **2008**, *20*, 4306.
(6) Eggins, B. R.; Irvine, J. T. S.; Murphy, E. P.; Grimshaw, J. *J. Chem. Soc., Chem. Commun.* **1988**, 1123.
(7) Kumar, A.; Kumar, S. *J. Phys. Org. Chem.* **1998**, *11*, 277.
(8) Shiragami, T.; Ankyu, H.; Fukami, S.; Pac, C.; Yanaglda, S.; Mori, H.; Fujita, H. *J. Chem. Soc., Faraday Trans.* **1992**, *88*, 1055.
(9) Inoue, H.; Yamachika, M.; Yoneyama, H. *J. Chem. Soc., Faraday Trans.* **1992**, *88*, 2215.
(10) Yanagida, S.; Shindo, A.; Hosokawa, H.; Mori, H.; Sakata, T.; Wada, Y.; Ogata, T. *Bull. Chem. Soc. Jpn.* **1995**, *68*, 752.
(11) Pal, B.; Torimoto, T.; Iwasaki, K.; Shibayama, T.; Takahashi, H.; Ohtani, B. *J. Phys. Chem. B* **2004**, *108*, 18670.
(12) Hosokawa, H.; Wada, Y.; Murakoshi, K.; Sakata, T.; Mori, H.; Yanagida, S.; Ogata, T. *J. Chem. Soc., Faraday Trans.* **1996**, *92*, 4575.
(13) Hoffman, A. J.; Mills, G.; Yee, H.; Hoffmann, M. R. *J. Phys. Chem.* **1992**, *96*, 5546.
(14) Kuehnel, M. F.; Wakerley, D. W.; Orchard, K. L.; Reisner, E. *Angew. Chem., Int. Ed.* **2015**, *54*, 9627.
(15) Nedeljkovic, J. M.; Nenadovic, M. T.; Micic, O. I.; Nozik, A. J. *J. Phys. Chem.* **1986**, *90*, 12.
(16) Kisch, H. *Angew. Chem., Int. Ed.* **2013**, *52*, 812.
(17) Chen, X. B.; Shen, S. H.; Guo, L. J.; Mao, S. S. *Chem. Rev.* **2010**, *110*, 6503.
(18) Osterloh, F. E. *Chem. Mater.* **2008**, *20*, 35.
(19) Wilker, M. B.; Schnitzenbaumer, K. J.; Dukovic, G. *Isr. J. Chem.* **2012**, *52*, 1002.
(20) Harris, L. A.; Wilson, R. H. *Annu. Rev. Mater. Sci.* **1978**, *8*, 99.
(21) Chaudhary, Y. S.; Woolerton, T. W.; Allen, C. S.; Warner, J. H.; Pierce, E.; Ragsdale, S. W.; Armstrong, F. A. *Chem. Commun.* **2012**, *48*, 58.
(22) Huang, J.; Mulfort, K. L.; Du, P. W.; Chen, L. X. *J. Am. Chem. Soc.* **2012**, *134*, 16472.
(23) Zhu, H. M.; Song, N. H.; Lv, H. J.; Hill, C. L.; Lian, T. Q. *J. Am. Chem. Soc.* **2012**, *134*, 11701.
(24) Yu, W. L.; Noureldine, D.; Isimjan, T.; Lin, B.; Del Gobbo, S.; Abulikemu, M.; Hedhili, M. N.; Anjum, D. H.; Takanabe, K. *Phys. Chem. Chem. Phys.* **2015**, *17*, 1001.
(25) Gimbert-Surinach, C.; Stoll, T.; Fortage, J.; Collomb, M. N.; Deronzier, A.; Palomares, E.; Llobet, A.; Albero, J. *J. Am. Chem. Soc.* **2014**, *136*, 7655.
(26) Li, Z. J.; Wang, J. J.; Li, X. B.; Fan, X. B.; Meng, Q. Y.; Feng, K.; Chen, B.; Tung, C. H.; Wu, L. Z. *Adv. Mater.* **2013**, *25*, 6613.
(27) Han, Z. J.; Qiu, F.; Eisenberg, R.; Holland, P. L.; Krauss, T. D. *Science* **2012**, *338*, 1321.
(28) Liu, C.; Qiu, F.; Peterson, J. J.; Krauss, T. D. *J. Phys. Chem. B* **2015**, *119*, 7349.
(29) Meng, P.; Wang, M.; Yang, Y.; Zhang, S.; Sun, L. *J. Mater. Chem. A* **2015**, *3*, 18852.
(30) Shemesh, Y.; Macdonald, J. E.; Menagen, G.; Banin, U. *Angew. Chem., Int. Ed.* **2011**, *50*, 1185.
(31) Brown, K. A.; Dayal, S.; Ai, X.; Rumbles, G.; King, P. W. *J. Am. Chem. Soc.* **2010**, *132*, 9672.
(32) Brown, K. A.; Wilker, M. B.; Boehm, M.; Dukovic, G.; King, P. W. *J. Am. Chem. Soc.* **2012**, *134*, 5627.
(33) Wang, F.; Wang, W.-G.; Wang, X.-J.; Wang, H.-Y.; Tung, C.-H.; Wu, L.-Z. *Angew. Chem., Int. Ed.* **2011**, *50*, 3193.
(34) Liang, W.-J.; Wang, F.; Wen, M.; Jian, J.-X.; Wang, X.-Z.; Chen, B.; Tung, C.-H.; Wu, L.-Z. *Chem. - Eur. J.* **2015**, *21*, 3187.
(35) Greene, B. L.; Joseph, C. A.; Maroney, M. J.; Dyer, R. B. *J. Am. Chem. Soc.* **2012**, *134*, 11108.
(36) de Mello Donega, C.; Bode, M.; Meijerink, A. *Phys. Rev. B: Condens. Matter Mater. Phys.* **2006**, *74*, 085320.
(37) Knowles, K. E.; Malicki, M.; Parameswaran, R.; Cass, L. C.; Weiss, E. A. *J. Am. Chem. Soc.* **2013**, *135*, 7264.
(38) Cass, L. C.; Swenson, N. K.; Weiss, E. A. *J. Phys. Chem. C* **2014**, *118*, 18263.
(39) Peterson, M. D.; Jensen, S. C.; Weinberg, D. J.; Weiss, E. A. *ACS Nano* **2014**, *8*, 2826.
(40) Resch-Genger, U.; Grabolle, M.; Cavaliere-Jaricot, S.; Nitschke, R.; Nann, T. *Nat. Methods* **2008**, *5*, 763.
(41) ten Cate, S.; Sandeep, C. S. S.; Liu, Y.; Law, M.; Kinge, S.; Houtepen, A. J.; Schins, J. M.; Siebbeles, L. D. A. *Acc. Chem. Res.* **2015**, *48*, 174.
(42) Zhao, J.; Osterloh, F. E.; Holmes, M. A. *ACS Nano* **2013**, *7*, 4316−4325.
(43) Bernt, C. M.; DeMartino, A. W.; Pierri, A. E.; Levy, E. S.; Zigler, D. F.; Ford, P. C.; Burks, P. T. *J. Am. Chem. Soc.* **2014**, *136*, 2192.
(44) Li, X.-B.; Li, Z.-J.; Gao, Y.-J.; Meng, Q.-Y.; Yu, S.; Weiss, R. G.; Tung, C.-H.; Wu, L.-Z. *Angew. Chem., Int. Ed.* **2014**, *53*, 2085.
(45) Pal, B.; Torimoto, T.; Okazaki, K.; Ohtani, B. *Chem. Commun.* **2007**, 483.
(46) Warrier, M.; Lo, M. K. F.; Monbouquette, H.; Garcia-Garibay, M. A. *Photochem. Photobiol. Sci.* **2004**, *3*, 859.
(47) Eskandari, P.; Zand, Z.; Kazemi, F. *J. Photochem. Photobiol., A* **2014**, *274*, 7.
(48) Schrauben, J. N.; Hayoun, R.; Valdez, C. N.; Braten, M.; Fridley, L.; Mayer, J. M. *Science* **2012**, *336*, 1298.
(49) Hoffman, A. J.; Yee, H.; Mills, G.; Hoffmann, M. R. *J. Phys. Chem.* **1992**, *96*, 5540.
(50) Chauvire, T.; Gasparutto, D.; Ravanat, J.-L.; Lebrun, C.; Gromova, M.; Jouneau, P.-H.; Chauvin, J.; Gambarelli, S.; Maurel, V.; Mouesca, J.-M. *J. Phys. Chem. C* **2015**, *119*, 17857.
(51) Morris-Cohen, A. J.; Malicki, M.; Peterson, M. D.; Slavin, J. J. W.; Weiss, E. A. *Chem. Mater.* **2013**, *25*, 1155.
(52) Smith, W. H.; Bard, A. J. *J. Am. Chem. Soc.* **1975**, *97*, 5203.
(53) Frederick, M. T.; Weiss, E. A. *ACS Nano* **2010**, *4*, 3195.
(54) Berr, M. J.; Vaneski, A.; Mauser, C.; Fischbach, S.; Susha, A. S.; Rogach, A. L.; Jackel, F.; Feldmann, J. *Small* **2012**, *8*, 291.
(55) Amirav, L.; Alivisatos, A. P. *J. Am. Chem. Soc.* **2013**, *135*, 13049.
(56) Acharya, K. P.; Khnayzer, R. S.; O'Connor, T.; Diederich, G.; Kirsanova, M.; Klinkova, A.; Roth, D.; Kinder, E.; Imbo-den, M.; Zamkov, M. *Nano Lett.* **2011**, *11*, 2919.
(57) Iwasita, T. *Electrochim. Acta* **2002**, *47*, 3663.




DOI: 10.1021/jacs.5b11353
*J. Am. Chem. Soc.* 2016, 138, 1591−1600

(58) Forlano, P.; Olabe, J. A.; Magallanes, J. F.; Blesa, M. A. *Can. J. Chem.* **1997**, *75*, 9.
(59) Maldotti, A.; Andreotti, L.; Molinari, A.; Tollari, S.; Penoni, A.; Cenini, S. *J. Photochem. Photobiol., A* **2000**, *133*, 129.
(60) Li, Y.-P.; Cao, H.-B.; Liu, C.-M.; Zhang, Y. *J. Hazard. Mater.* **2007**, *148*, 158.
(61) Scifinder-calculated using ACD/Labs Software, Chemical Abstracts Service, 2015.
(62) Croston, M.; Langston, J.; T akacs, G.; Morrill, T. C.; Miri, M.; Santhanam, K. S. V.; Ajayan, P. *Int. J. Nanosci.* **2002**, *1*, 285.
(63) Hurley, R.; Testa, A. C. *J. Am. Chem. Soc.* **1966**, *88*, 4330.
(64) Haram, S. K.; Quinn, B. M.; Bard, A. J. *J. Am. Chem. Soc.* **2001**, *123*, 8860.
(65) Lund, H. *Organic Electrochemistry*; 4th ed.; Marcel Dekker: New York, 2001.
(66) Cass, L. C.; Malicki, M.; Weiss, E. A. *Anal. Chem.* **2013**, *85*, 6974.
(67) Malicki, M.; Knowles, K. E.; Weiss, E. A. *Chem. Commun.* **2013**, *49*, 4400.
(68) Knowles, K. E.; Peterson, M. D.; McPhail, M. R.; Weiss, E. A. *J. Phys. Chem. C* **2013**, *117*, 10229.
(69) Knowles, K. E.; McArthur, E. A.; Weiss, E. A. *ACS Nano* **2011**, *5*, 2026.
(70) McArthur, E. A.; Morris-Cohen, A. J.; Knowles, K. E.; Weiss, E. A. *J. Phys. Chem. B* **2010**, *114*, 14514.
(71) Cooney, R. R.; Sewall, S. L.; Dias, E. A.; Sagar, D. M.; Anderson, K. E. H.; Kambhampati, P. *Phys. Rev. B: Condens. Matter Mater. Phys.* **2007**, *75*, 245311.
(72) Klimov, V. I.; Schwarz, C. J.; McBranch, D. W.; Leatherdale, C. A.; Bawendi, M. G. *Phys. Rev. B: Condens. Matter Mater. Phys.* **1999**, *60*, R2177.
(73) Boulesbaa, A.; Stockwell, D.; Huang, Z.; Huang, J.; Guo, J.; Lian, T.; Issac, A. *J. Am. Chem. Soc.* **2007**, *129*, 15132.
(74) Morris-Cohen, A. J.; Frederick, M. T.; Cass, L. C.; Weiss, E. A. *J. Am. Chem. Soc.* **2011**, *133*, 10146.
(75) Zhu, H.; Yang, Y.; Hyeon-Deuk, K.; Califano, M.; Song, N.; Wang, Y.; Zhang, W.; Prezhdo, O. V.; Lian, T. *Nano Lett.* **2014**, *14*, 1263.
(76) Chi, Y.; Fu, H.; Qi, L.; Shi, K.; Zhang, H.; Yu, H. *J. Photochem. Photobiol., A* **2008**, *195*, 357.
(77) Korgel, B. A.; Monbouquette, H. G. *J. Phys. Chem. B* **1997**, *101*, 5010.
(78) Chang, C. M.; Orchard, K. L.; Martindale, B. C. M.; Reisner, E. *J. Mater. Chem. A* **2016**, DOI: 10.1039/C5TA04136H.
(79) Lee, J. M.; Ham, Y.; Kim, I. Y.; Domen, K.; Hwang, S.-J.; Gunjakar, J. L. *Chem. - Eur. J.* **2014**, *20*, 17004.
(80) Perera, D.; Lorek, R.; Khnayzer, R. S.; Moroz, P.; O'Connor, T.; Khon, D.; Diederich, G.; Kinder, E.; Lambright, S.; Castellano, F. N.; Zamkov, M. *J. Phys. Chem. C* **2012**, *116*, 22786.
(81) Huang, J.; Huang, Z.; Jin, S.; Lian, T. Q. *J. Phys. Chem. C* **2008**, *112*, 19734.


DOI: 10.1021/jacs.5b11353
*J. Am. Chem. Soc.* 2016, 138, 1591−1600